Test of photon strength functions by a method of two-step cascades

F. Bečvář and P. Cejnar
Charles University, Faculty of Mathematics and Physics, Prague 8, CS-18000, Czechoslovakia

R. E. Chrien
Brookhaven National Laboratory, Upton, New York 11973

J. Kopecký
Nederlands Energy Research Foundation ECN, P.O.Box 1, 1755 ZG Petten, The Netherlands
(Received 5 February 1992)

The applicability of sum-coincidence measurements of two-step cascade γ-ray spectra for the determination of photon strength functions is discussed. The method is sensitive, not only to primary transitions, but also to secondary transitions proceeding from states of intermediate excitation. An experiment based on thermal neutron capture in a Nd target was undertaken at the Brookhaven National Laboratory High Flux Beam Reactor to test various hypotheses of $E1$ and $M1$ photon strength function in the ^{144}Nd nucleus. The results were compared to a series of model calculations, in which the back-shifted Fermi gas model is used to represent the level density. Models derived from the Fermi theory of liquids are strongly preferred.

PACS numbers: 25.40.Lw, 27.60.+j, 21.10.Pc

I. INTRODUCTION

Giant dipole resonances, observed since 1947 in the cross section of photonuclear reactions [1], have been explained as dipole vibrations of proton and neutron liquids in the nucleus [2]. The intuitive concept of the independence of this collective motion from intrinsic nuclear excitations results in the important consequence that giant resonances built on the ground state as well as those built on any excited state have the same size and shape. This assumption, first stated by Brink [3] in 1955, is called Brink's hypothesis.

Using Brink's hypothesis and assuming the principle of detailed balance, one can find a relationship between the smoothed $E1$ part of the photoexcitation cross section and the average value of partial radiation widths for the inverse process of the $E1$ photodeexcitation [4]. Let us designate the smoothed $E1$ part of the photoabsorption cross section at the γ-ray energy E_γ as $\overline{\sigma}_{E1}(E_\gamma)$, and the average partial radiation width of $E1$ transitions from states with spin and parity J^π and energy E to a state $J'^{\pi'}$ at energy $E' = E - E_\gamma$ as $\overline{\Gamma}_\gamma(J^\pi E \rightarrow J'^{\pi'} E')$. The relationship can then be written in the following form:

$$\frac{1}{3\pi^2(\hbar c)^2}\,\frac{1}{E_\gamma}\,\overline{\sigma}_{E1}(E_\gamma) = \frac{\overline{\Gamma}_\gamma(J^\pi E \rightarrow J'^{\pi'} E')\;\rho(J^\pi, E)}{E_\gamma^3} \equiv S_{E1}(E_\gamma)\ . \quad (1)$$

Here $\rho(J^\pi, E)$ is the density of levels with spin and parity J^π at energy E. The right-hand side of Eq. (1) is identical with what is usually called the $E1$ strength function $S_{E1}(E_\gamma)$. In Eq. (1) it is assumed that $S_{E1}(E_\gamma)$ is independent of spin.

The other components of the photoabsorption cross section, corresponding to other types and multipolarities of the electromagnetic radiation, can be subjected to a quite similar procedure and, as a consequence, we can define the photon strength function $S_{XL}(E_\gamma)$ for the radiation of type X and multipolarity L. Conventionally, in the general case, the factor E_γ^{2L+1} occurs in the denominator of the definition of $S_{XL}(E_\gamma)$ instead of E_γ^3.

A consequence of Brink's hypothesis is that the photon strength function defined above for photodeexcitation is independent of the properties of the final state, and is a function only of the variable E_γ. It is in this sense that we refer to models which depend on properties of *both* final and initial states in a deexcitation as those inconsistent with Brink's hypothesis.

Most data on photoabsorption cross sections support a Lorentzian shape for the $E1$ strength function. Such a shape follows from simple semiclassical models. However, radiation widths of neutron resonances for transitions to low-lying states are overestimated typically by a factor of three in this model [3]. Therefore, the simple Lorentzian shape of the giant dipole resonance (GDR) may be inadequate at energies close to the neutron binding energy and, consequently, more complex models have been proposed. Dover, Lemmer, and Hahn [5] pointed out that the damping width of the Lorentzian must be dependent on excitation energy. McCullagh, Stelts, and Chrien [6] achieved better agreement with experimental data for electric dipole transitions using an energy-dependent damping width.

Up to now, a great deal of information on the $E1$ strength function at energies close to the neutron binding energy has been accumulated from thermal and resonance neutron experiments [4]. Most of the strength function data obtained by an application of Brink's hypothesis have been for "hard" γ rays. Relatively little

information has been available for "soft" γ rays following capture. However, information on α-particle spectra from thermal [7] and resonant capture [8] of neutrons has been interpreted to indicate a sizable soft primary photon strength from the $(n, \alpha\gamma)$ reaction. This result is not consistent with a literal application of Brink's hypothesis, since in any of the above formulations with fixed or energy-dependent damping widths, the electric dipole strength function approaches zero as the photon energy approaches zero.

Kadmenskij, Markushev, and Furman [9] recognized that the $E1$ strength function has a nonzero limit for $E_\gamma \rightarrow 0$, based on the analytic properties of the dipole polarization operator. They developed a suitable approximation for the low-energy limit. Starting from the Fermi theory of liquids, they predicted that the damping width should also depend on the temperature of the state on which the GDR is built. $S_{E1}(E_\gamma)$ is modified, so that

$$S_{E1}(E_\gamma) \rightarrow S_{E1}(E_\gamma, T(E')) \ .$$

Independently, Zaretski and Sirotkin [10, 11] have developed a similar formulation.

These properties imply that the strength function cannot be written as a function of the transition energy alone, and constitutes a major modification of the Brink hypothesis.

The method of two-step cascades, proposed by Hoogenboom [12] more than 30 years ago, has been used to study neutron radiative capture in the past. This method has been exploited in a series of experiments by Popov and his collaborators [13]. In the present paper we demonstrate that this method can provide indirect evidence for electric and magnetic dipole transition strengths in an intermediate excitation region, approximately midway between the capture state and the low-lying states of a nucleus. We also show how this evidence requires a modification of Brink's hypothesis. Results obtained with the nuclide ^{144}Nd are shown.

II. THE METHOD

A. Idea

The method is based on a two-detector coincidence measurement of γ transitions following thermal neutron capture. Each individual event in this measurement can be characterized by amplitudes of both detector signals and by their time difference. Those events for which coincident detector signals correspond to a fixed energy sum are of special interest. By selecting an energy sum equal to the energy difference between the capturing state and a low-lying state, we can study two-step cascades connecting the capturing state and a fixed low-lying state. The spectrum of energies deposited in one detector for those events in which the condition of the coincidence is fulfilled as well as the condition on the energy sum contains all transition energies involved in a two-step cascade deexcitation process.

The coincidence spectrum inherently contains a background caused by the Compton effect and by accidental coincidences. Two γ rays with the energy sum exceeding the adjusted energy sum can produce a spurious event if the surplus energy escapes after the Compton interaction. In a similar way, two γ rays, this time with the right value of the energy sum but originating from two different neutron captures, can be accidentally detected at the same time and also produce a spurious event.

In order to eliminate this background we extract coincidence spectra by a special scanning procedure. Eight rectangular regions that surround the peak corresponding to a preselected final state, at which two-step cascades terminate, are defined in the (energy-sum) $\times$ (detection-time-difference) plane. These regions are used to provide the background correction for the coincidence spectrum, corresponding to a given final state. The background correction is derived from a superposition of eight coincidence spectra surrounding the region of interest. The coincidence spectrum corrected for the background determined by this procedure is called the two-step cascade (TSC) spectrum.

The TSC spectrum consists of a great number of lines. Among them only those corresponding to cascades proceeding via low-energy intermediate states are well separated. The others, corresponding to cascades via intermediate states with higher energy (above ≈ 3 MeV), give rise to an unresolved quasicontinuum. This quasicontinuum forms a gross structure with a maximum in the middle of the TSC spectrum. The shape and size of this component of the TSC spectrum carry information on the photon strength function that governs the emission of γ rays in the deexcitation process. The TSC spectrum for each low-energy level can be examined and a comparison of these spectra with those obtained in modeling with various hypotheses of photon strength functions and level densities makes it possible to study the behavior of photon strength functions at intermediate energies.

B. "Parasitic" phenomena

Because the detectors do not distinguish between the primary and the secondary γ rays, the TSC spectra behave as if they came from a spectrometer whose energy response function is characterized by two peaks placed symmetrically with respect to the midpoint of the spectrum. After correction for energy-dependent detector efficiencies the TSC spectrum displays this symmetry, modified by the energy variation of the detector resolution.

Under close scrutiny the TSC spectra are, in fact, even more complicated than is implied by the above analysis. Besides the two main peaks each two-step cascade gives rise to additional small structures in the TSC spectrum. These can be understood as follows. Consider two γ rays emitted in a cascade. The first γ ray, for example, can be detected in one of the detectors, scattered back to the other detector and detected there together with the second γ ray. In this process the full energy of these γ rays is distributed between the two detectors so that the condition of the energy sum is clearly fulfilled as in the case of separate detection of two γ rays in each detector. A similar situation may occur when the energy exchange

between detectors is not provided via backscattering but via bremsstrahlung or annihilation γ quanta.

Following the reasoning outlined above, the following distortions, which may be termed "crosstalk," can be categorized: (i) Compton backscattering leads to a pair of satellite structures which accompany each main peak in the spectrometer response function on its left- and right-hand sides. Multiple Compton scattering results in a broad background in a vicinity of both peaks. (ii) An interchange of annihilation photons leads to two pairs of satellite peaks both differing by $\pm$ 511 keV from the main peak. (iii) An annihilation photon originating in one of detectors can undergo a Compton scattering in this detector. This process contributes to a continuous background between the main peak and its annihilation satellites. (iv) A bremsstrahlung photon radiated by an electron or positron from an interaction of a γ ray in one of the detectors can be absorbed in the second detector. As a result, two wide satellite peaks arise near the main peaks. These satellites are believed to be small, however, compared to those originating from Compton scattering. (v) Effects of higher order, in which more exchanges are realized, are also present in the TSC spectrum. However, the probability of a multiple exchange strongly decreases with multiplicity because of low photon detection efficiency.

Satellite structures accompany each peak in the discrete part of the TSC spectrum as well as in the quasicontinuum. Their contribution can be partly reduced by an absorber placed between the detectors. We used another method, based not on a prevention of exchange effects, but on the determination of the size of their contribution in the TSC spectra observed. The relative size of the satellites varies smoothly with the primary photon energy and we are able to use satellites of strong and well-separated lines for an estimate of the contribution of exchange effects to the quasicontinuum component of the TSC spectrum.

Because of exchange effects, the process of direct deexcitation of the capturing state to the final state selected also contributes to the TSC spectrum. In that case the energy of the exchanged quantum is deposited in one detector while *all* the remaining energy of the cascade is deposited in the other detector. Additional backscatter, annihilation, and bremsstrahlung structures at the beginning and end of the TSC spectrum arise as a consequence.

Processes of n-step deexcitation of the capturing state ($n > 2$) occur in the TSC spectrum if several photons are detected by one detector in time coincidence. On the one hand, the probability of the simultaneous detection of more photons decreases with the number of photons; on the other hand, the probability of the deexcitation by three-step (or more) cascades may be higher than that for two-step cascades. Therefore, the contribution of three-step cascades in the TSC spectrum may be considerable and must be accounted for.

The effects of "vetoing" must also be considered. Vetoing occurs due to a γ decay of the final state selected. When photons from a two-step (or three-step) cascade to the final state are fully absorbed, photons from following transitions can be simultaneously detected and eliminate the event from the TSC spectrum by the perturbation of the energy sum. Consequently, TSC intensities, except those to the ground state, are reduced. This effect can be strong even for low-lying final states. An estimate of vetoing corrections is possible if the energy dependence of the absolute detection efficiency is known for both detectors. From the low-lying states with known branching ratios we can calculate corrections using detection probabilities for transitions between these states. In these corrections we neglect angular correlations.

III. EXPERIMENT

A sample of natural Nd was irradiated in a beam of thermal neutrons at the Brookhaven National Laboratory High Flux Beam Reactor for about 300 h. For elemental neodymium, most of the thermal neutron capture (about 80%) occurs on ^{143}Nd to form 3^- and 4^- capturing states in ^{144}Nd.

Two face-to-face HPGe detectors with overall photopeak efficiency of 1.95% and 2.30% at 696 keV (including the effect of solid angle) were used (Fig. 1). Digital information on γ-ray energies and detection time differences for each individual event were accumulated on magnetic tape. The spectrum of the energy sums reconstructed from all accumulated events is represented in Fig. 2. As the channel number scale of each detector is not a strictly linear function of γ-ray energy, both channel scales had to be linearized using a simple rebinning procedure. As a result, the spectrum of energy sums has a linear scale. The resulting number of count in each channel of this spectrum was additionally randomized to avoid correlations between neighboring channels.

The data accumulated were later scanned off-line by the procedure described in Sec. II A to yield the TSC spectra for five lowest final states in ^{144}Nd: the 0^+ ground state, the 2^+ state at 696 keV, the 4^+ state at 1314 keV, the 3^- state at 1510 keV, and the 2^+ state at 1561 keV. The scanning procedure also incorporated linearization

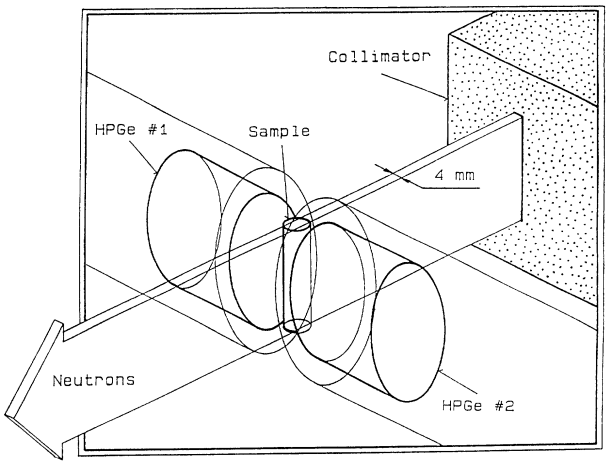

FIG. 1. The geometry of the sum-coincidence measurement.

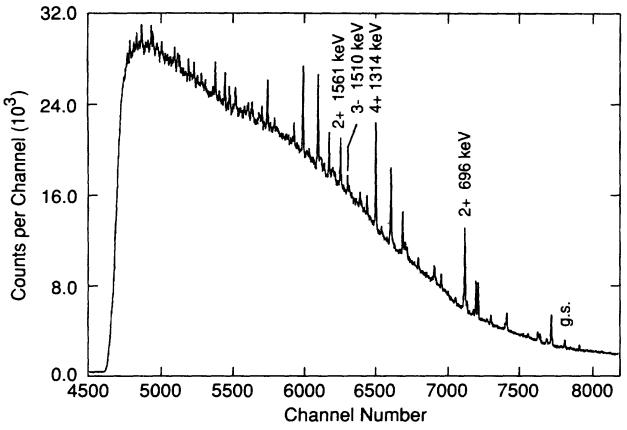

FIG. 2. The spectrum of γ-ray energy sums in the two-detector coincidence measurement with the Nd target. Peaks corresponding to cascades feeding the five low-energy final states are indicated with their spin, parity, and excitation energy.

and randomization, as stated above. The linearization turned out to be important as it ensured good energy resolution in the formation of the energy sums in the scanning procedure. The energy resolution in the spectrum of energy sums shown in Fig. 2 is 6.9 keV, full width at half maximum (FWHM), at 7100 keV. For the TSC spectrum a resolution of 2.8 and 4.9 keV at energies of 600 and 7100 keV, repectively, was achieved. These resolutions include the effects of long-term instabilities.

The TSC spectra obtained were corrected for variation of detector efficiencies, determined from single-spectrum measurements with a NaCl target using the same geometry as that in coincidence measurements with the Nd target. The γ-ray intensities in the $^{35}\mathrm{Cl}(n,\gamma)^{36}\mathrm{Cl}$ reaction were taken from Ref. [14].

A separate thermal (n,γ) single-spectrum measurement with a mixed Nd+Cl target made it possible to determine an absolute intensity for the primary transition to the 4^+ state at 1314 keV in ^{144}Nd nucleus as 7.36%. Using this value and the fact that the decay branching ratio of the 4^+ state at 1314 keV for the transition to the 2^+ state at 696 keV is close to 100%, we establish an absolute intensity scale for the TSC spectra.

An example of a TSC spectrum is given in Fig. 3. A

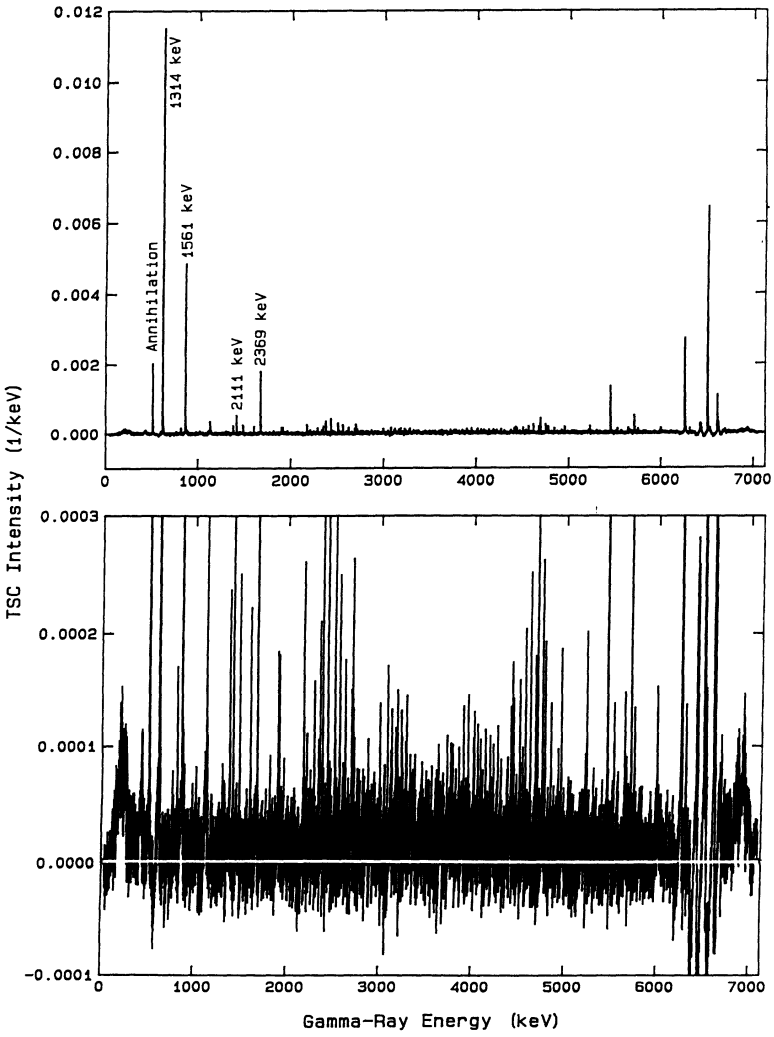

FIG. 3. The TSC spectrum for the 2^+ state at 696 keV in the ^{144}Nd nucleus, corrected for detector energy efficiency variation. The vertical scale in the lower half has been expanded to show the quasicontinuum component more clearly. The energies of the intermediate states corresponding to the strongest lines are indicated.

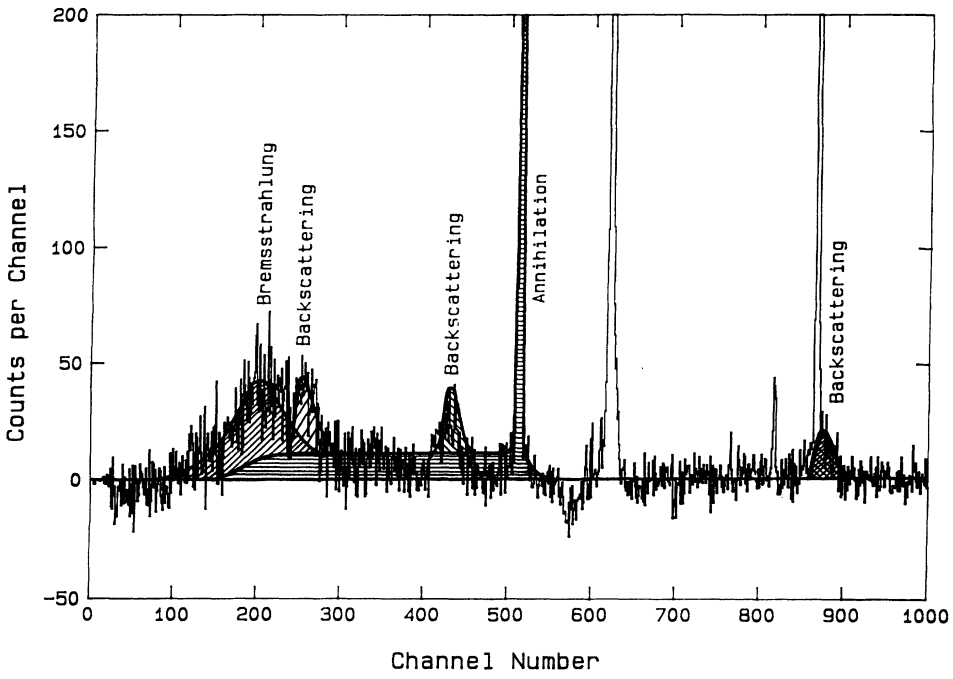

FIG. 4. Parasitic phenomena in the TSC spectrum for the 2^+ final state at 696 keV. In contrast to Fig. 3 no efficiency corrections are included. The structures due to bremsstrahlung, annihilation, and backscattering are very strong in the region shown, from 0 to 1 MeV. Both kinds of backscatter peaks are shown, those present always at the beginning of the spectrum (shown at the left) and those accompanying each two-step cascade peak in the TSC spectrum as satellites (the two at the right).

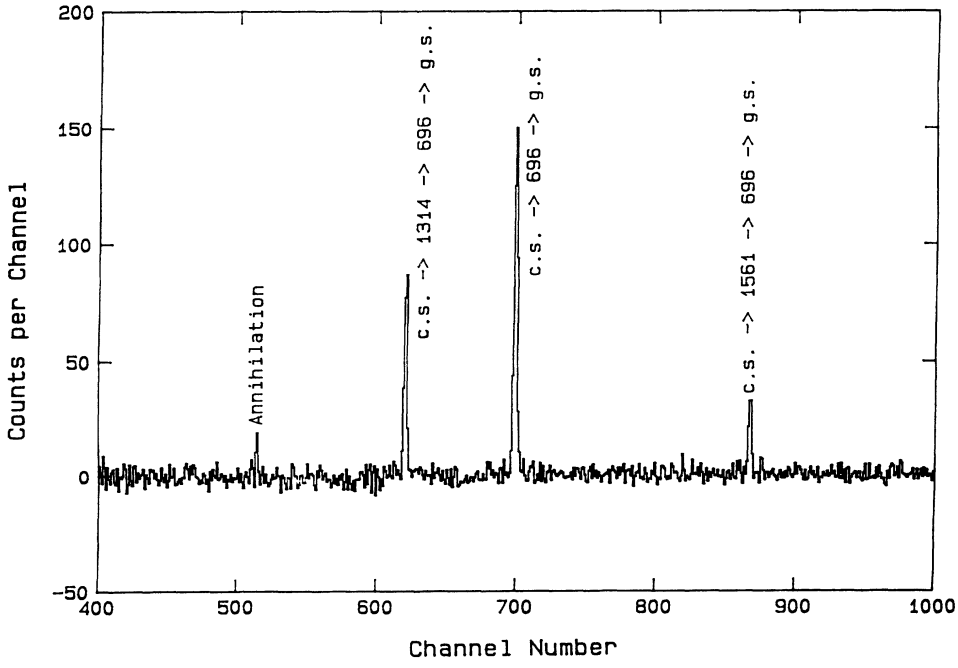

FIG. 5. Manifestation of three-step cascades in the TSC ground state spectrum. Two peaks corresponding to the three-step cascades (capture state → 1314 keV → 696 keV → g.s.) and (capture state → 1561 keV → 696 keV→ g.s.) are indicated, as well as the peak of a two-step cascade via the intermediate state at 696 keV.

global view of the spectrum represented in the upper part of the figure and the lower part details a large number of well-separated lines. In this figure, the TSC intensity of the strongest line, corresponding to the cascade via the 4^+ intermediate state at 1314 keV, is stronger than the mean of the other well-separated lines by a factor of about 100, illustrating the violent Porter-Thomas fluctuations of transition intensities. The quasicontinuum component of the TSC spectrum, shown in the lower part of the figure, is statistically significant and its overall integrated TSC intensity is comparable to the intensities of the strongest lines in the TSC spectrum. Undershoots accompanying strong peaks, evident in the figure, are well understood as an attribute of the scanning procedure used (see the explanation in Ref. [15]). Figure 4 illustrates the parasitic structures described in the previous section. Although such structures are not evident in the quasicontinuum portion of the spectrum, it is important to understand such structures to establish the validity of the method.

The quasicontinuum part of the TSC spectra displays large intensity fluctuations due to Porter-Thomas statistics and experimental uncertainties. Because of intensity fluctuations, a comparison of the observed TSC spectra with those obtained in modeling must be carried out over a reasonably wide range of integration over energy. Such a range should include a sufficient number of transitions, but at the same time it should not include those transitions that strongly dominate the TSC spectrum. In this case, the fluctuations cannot perturb the model comparisons. We integrated the TSC spectrum over an energy interval of 2.4 MeV situated symmetrically in the middle of the TSC spectrum. The integrated TSC intensities could be determined with a statistical accuracy of 9.7, 2.6, 6.8, 7.2, and 12.4 % for our five final states at 0, 696, 1314, 1510, and 1561 keV, respectively. Besides these uncertainties a systematic error of about 16%, following from the normalizing procedure, is present.

All these integrated TSC intensities were corrected for exchange effects described in Sec. II B, using the extraordinarily strong cascade to the 2^+ state at 696 keV via the 4^+ state at 1314 keV, for which backscattering and annihilation satellites in the TSC spectrum can be readily recognized (Fig. 4). These corrections are relatively small: their overall size is about 6%. Corrections for the effect of vetoing are represented by factors ranging from 0.73 to 1.39 (the fact that the correction can be less than one follows from the normalization procedure). No corrections were done for bremsstrahlung (Fig. 4) because its contribution to the useful part of a TSC spectrum is expected to be small, not higher than 2%.

Figure 5 demonstrates the presence of three-step cascades in the experimental TSC spectra. A comparison of the intensity of the line corresponding to the three-step cascade (capture state $\rightarrow$ 1314 keV$\rightarrow$ 696 keV $\rightarrow$g.s.) in the ground state TSC spectrum with the line corresponding to the two-step cascade (capture state $\rightarrow$ 1314 keV $\rightarrow$ 696 keV) in the TSC spectrum for the 696 keV state made it possible to determine the absolute detector efficiencies. As explained above, it is important to account for the three-step cascade components in TSC spectra.

IV. MODELING PROCEDURE

As described above the integrated TSC intensities in the defined range of the quasicontinuum part of the spectrum were evaluated for five lowest final states in the ^{144}Nd nucleus. These intensities are expressed as number of events, per captured neutron, in the selected interval . In order to test various hypotheses about photon strength functions we modeled the TSC process and compared the resulting integrated TSC intensities with those observed experimentally.

There are two ways to calculate expected TSC intensities. The more straightforward one is based on the Monte Carlo method. A randomly created set of nuclear levels and a set of all partial radiation widths for γ transitions from each level are constructed under the constraints of the model and Porter-Thomas statistics. The branching ratio for decay of a level 1 to a level 2 is

$$P(1 \rightarrow 2) = \frac{\Gamma_\gamma(1 \rightarrow 2)}{\Gamma_\gamma(1)} \quad , \tag{2}$$

where $\Gamma_\gamma(1 \rightarrow 2)$ is the partial radiation width and $\Gamma_\gamma(1)$ is the total radiation width of the level 1 given by

$$\Gamma_\gamma(1) = \sum_k \Gamma_\gamma(1 \rightarrow k) \quad . \tag{3}$$

By the generation of random two- and three-step cascades with probabilities equal to the appropriate products of probabilities from Eq. (2), multiplied by detection probabilities, we get a realization of the TSC spectrum corresponding to the model selected. Varying the sets of levels and their partial radiation widths under a given model, we can obtain average values and the correlation matrix of all integrated TSC intensities. This method would make it possible to take into account all correlations between integrated TSC intensities exactly. However, in the case of three-step cascades it would be rather awkward computationally. We have chosen a simpler method, which is in our opinion adequate, considering the approximate character of models of photon strength functions elaborated so far.

The main feature of this simpler method is the use of quantities averaged over many levels. From the right-hand side of Eq. (1), modified for transition type and multipolarity, the average value of the total radiation width of a state with spin and parity J^π at excitation energy E can be expressed as

$$\overline{\Gamma}_\gamma(J^\pi, E) = \frac{1}{\rho(J^\pi, E)} \sum_{J'\pi'} \sum_{XL} \int_0^E S_{XL}(E - E', T(E'))(E - E')^{2L+1} \rho(J'^{\pi'}, E')\, dE' \quad , \tag{4}$$

where XL are the multipolarites of transitions that can connect the state (E, J^π) with the state $(E', J'^{\pi'})$. We have taken into account $XL = E1$, $M1$, and $E2$ contributions only. An estimate of an average decay branching ratio of the state $J^\pi E$ for the transition to a state $J'^{\pi'} E'$ is given by the expression

$$\overline{P}(J^\pi E \to J'^{\pi'} E') \approx \frac{\overline{\Gamma}_\gamma(J^\pi E \to J'^{\pi'} E')}{\overline{\Gamma}_\gamma(J^\pi, E)} \quad , \tag{5}$$

where the average partial radiation width in the numerator is evaluated from the general XL modification of the right-hand side of Eq. (1). Equation (5) holds as long as there is only a small dispersion in the total radiation width.

For the total probability of decays of the capturing state $J_c^{\pi_c} E_c$ by two-step cascades via intermediate states $J_1^{\pi_1}$ in the infinitesimal energy interval dE_1 at E_1 to the final state $J_f^{\pi_f} E_f$ we get

$$\approx \overline{P}(J_c^{\pi_c} E_c \to J_1^{\pi_1} E_1)\rho(J_1^{\pi_1}, E_1)\overline{P}(J_1^{\pi_1} E_1 \to J_f^{\pi_f} E_f)dE_1 \tag{6}$$

and analogous decays by three-step cascades have the total probability

$$\approx \overline{P}(J_c^{\pi_c} E_c \to J_1^{\pi_1} E_1)\rho(J_1^{\pi_1}, E_1)\overline{P}(J_1^{\pi_1} E_1 \to J_2^{\pi_2} E_2)\rho(J_2^{\pi_2}, E_2)\overline{P}(J_2^{\pi_2} E_2 \to J_f^{\pi_f} E_f)dE_1 dE_2 \quad . \tag{7}$$

In order to evaluate a TSC intensity we sum these probabilities over all intermediate spins and parities accessible by $E1$ or $M1$ or $E2$ transitions with respect to the restriction already described, multiply them by appropriate detection probabilities, and integrate them over the region of excitation energies to give the contribution to the desired part of the TSC spectrum. This integration is simple for two-step cascades component of TSC spectra, because only two ways of detecting two-step cascade are possible (the primary photon to the first detector, the secondary photon to the second detector, and the opposite). Expressing for example the two-step component of a TSC spectrum between energies ε_1 and ε_2, we have to integrate over both intervals $(E_c - \varepsilon_2, E_c - \varepsilon_1)$ and $(E_f + \varepsilon_1, E_f + \varepsilon_2)$ of the intermediate level energy. For three-step components of the TSC spectrum there are six regions in the $E_1 \times E_2$ plane over which integration has to be carried out; each corresponds to one way of detection of three photons by two detectors.

For the dispersion $\overline{\Delta^2\Gamma_\gamma}(J^\pi E \to J'^{\pi'} E')$ of partial radiation widths of the transition $J^\pi E \to J'^{\pi'} E'$ the Porter-Thomas distribution gives the relative dispersion

$$\frac{\overline{\Delta^2\Gamma_\gamma}(J^\pi E \to J'^{\pi'} E')}{:\overline{\Gamma}_\gamma(J^\pi E \to J'^{\pi'} E'):^2} = 2 \tag{8}$$

and hence the absolute dispersion of the total radiation widths is

$$\overline{\Delta^2\Gamma_\gamma}(J^\pi, E)$$

$$= 2\sum_{J',\pi'} \int_0^E :\overline{\Gamma}_\gamma(J^\pi E \to J'^{\pi'} E'):^2 \rho(J'^{\pi'}, E')dE' \quad . \tag{9}$$

An estimate of dispersions of quantities given by Eqs. (6) and (7) enables us to determine the dispersion of the integrated TSC intensity. However, various correlations are neglected in this method and resulting dispersions can be regarded only as first approximations.

V. HYPOTHESES TESTED

A. Level density

The back-shifted Fermi gas model in the form taken from Dilg *et al.* [16] was employed in our model calculations. According to this model the density of levels with spin I at the excitation energy E is

$$\rho(E, I) = \frac{1}{24\sqrt{2}} \frac{2I+1}{\sigma^3 a^{\frac{1}{4}}} \times \frac{\exp[2a^{\frac{1}{2}}(E-\Delta)^{\frac{1}{2}} - I(I+1)/2\sigma^2]}{(E-\Delta+T)^{\frac{5}{4}}} \quad . \tag{10}$$

Here a is the single-particle level density parameter, Δ is the backshift, T is the nuclear temperature, satisfying

$$E - \Delta = aT^2 - T \quad , \tag{11}$$

and σ is the spin cutoff parameter, given by the expression

$$\sigma^2 = \frac{\mathcal{J}T}{\hbar^2} \quad , \tag{12}$$

where $\mathcal{J}$ is the nuclear moment of inertia. From Eq. (10) the total state density of Lang and LeCoteur [17] can be derived.

Two empirical limits of the nuclear moment of inertia

$$\mathcal{J} = \mathcal{J}_{\text{rig}} \approx 0.0150 A^{\frac{5}{3}} \ \hbar^2 \,\text{MeV}^{-1} \tag{13}$$

and

$$\mathcal{J} = \tfrac{1}{2}\ \mathcal{J}_{\text{rig}} \approx 0.0075 A^{\frac{5}{3}} \ \hbar^2 \,\text{MeV}^{-1} \tag{14}$$

have been employed in our calculations. For these two cases the parameters a and Δ were adjusted separately using data on low-energy levels and on neutron s-resonance spacing. We get the following results, which are in good agreement with systematics [16]:

(LD-a) for $\mathcal{J} = \mathcal{J}_{\rm rig}$, $a = 15.82$ MeV^{-1},

$\Delta = 0.998$ MeV ,

(LD-b) for $\mathcal{J} = \frac{1}{2}\,\mathcal{J}_{\rm rig}$ $a = 14.58$ MeV^{-1},

$\Delta = 0.968$ MeV.

In a previous analysis [20] we employed another model of the level density, represented for low energies by the simple exponential function (constant temperature formula). However, in Refs. [18] and [19], generally better agreement of the model calculations with experimental results was obtained for the back-shifted Fermi gas model. It should be noted that parameters a and Δ differ from those used earlier [18, 19] because of a different value used for the neutron s-resonance spacing; here it is assumed to be 32 eV [21].

B. Photon strength functions

1. $E1$ radiation

We have tested the following forms for $E1$ strength functions. The comparison of these models is shown graphically in Fig. 6, for the case of ^{144}Nd.

($E1$-a) The standard Lorentzian

$$S_{E1}(E_\gamma) = \frac{1}{3\pi^2(\hbar c)^2}\,\sigma_0\,\frac{E_\gamma \Gamma_G^2}{(E_\gamma^2 - E_G^2)^2 + E_\gamma^2 \Gamma_G^2}\ , \qquad (15)$$

where the energy and the damping width of the giant resonance [22]

$E_G = 15.05$ MeV ,

$\Gamma_G = 5.30$ MeV ,

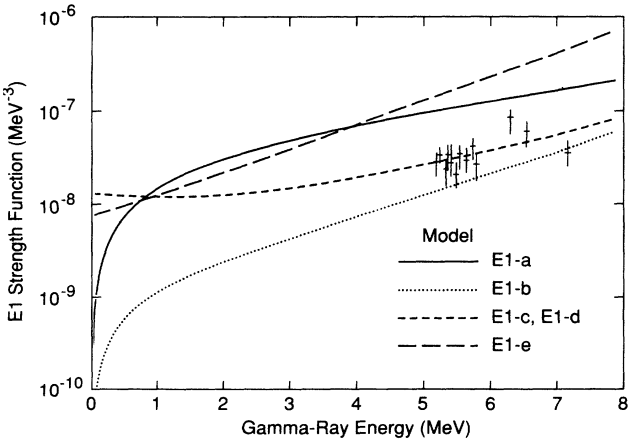

FIG. 6. A comparison of the various $E1$ strength function models for ^{144}Nd, with the initial state corresponding to thermal neutron capture. The models are identified in the text. The experimental data are taken from Ref. [6], which includes unpublished data of Raman [27].

and the photoabsorption cross section at $E_\gamma = E_G$

$\sigma_0 = 0.317$ b .

($E1$-b) The Lorentzian with an energy- and temperature-dependent damping width [23]

$$S_{E1}(E_\gamma, T) = \frac{1}{3\pi^2(\hbar c)^2}\sigma_0 \frac{E_\gamma \Gamma_G\, \Gamma(E_\gamma, T)}{(E_\gamma^2 - E_G^2)^2 + E_\gamma^2\, \Gamma(E_\gamma, T)^2}\ , \qquad (16)$$

where the damping width

$$\Gamma(E_\gamma, T) = \frac{\Gamma_G}{E_G^2}(E_\gamma^2 + 4\pi^2 T^2)\ . \qquad (17)$$

Because the right-hand side of Eq. (16) contains explicitly the nuclear temperature T, the $E1$ strength function depends not only on the transition energy E_γ, but also on the final state energy E_f (or on the initial state energy $E_i = E_f + E_\gamma$). As a consequence, the $E1$ strength function following Eq. (16) has a more complicated form than that usually associated with Brink's hypothesis. The temperature has been determined from Eq. (11).

The first term of Eq. (17) follows from a spreading of particle-hole states into more complex states, while the second term, derived from the Fermi theory of liquids, takes into account collisions between quasiparticles. The factor Γ_G/E_G^2 in Eq. (17) ensures the smooth transition of Eq. (16) to Eq. (15) for $T \to 0$ and $E_\gamma \to E_G$.

($E1$-c) The model by Kadmenskij *et al.* [9]

$$S_{E1}(E_\gamma, T) = \frac{1}{3\pi^2(\hbar c)^2}\,\sigma_0 \left(\frac{1 + \frac{2}{3}f_1'}{1 + 2f_1}\right)^{\frac{1}{2}} \times \frac{E_G\, \Gamma_G\, \Gamma(E_\gamma, T)}{(E_\gamma^2 - E_G^2)^2}\ , \qquad (18)$$

where f_1 and f_1' are parameters of a quasiparticle interaction. In accordance with the original paper we take

$$\left(\frac{1 + \frac{2}{3}f_1'}{1 + 2f_1}\right)^{\frac{1}{2}} = 0.7\ .$$

This model is based on an approximation from the Fermi theory of liquids for $E_\gamma \ll E_G$. It should be noted that this model incorporates the correct low-energy limiting behavior of the electric dipole operator, and Eq. (18) leads to a nonzero limit for $E_\gamma \to 0$:

$$\lim_{E_\gamma \to 0} S_{E1}(E_\gamma, T) = \frac{1}{3\pi^2(\hbar c)^2} \times \sigma_0 \left(\frac{1 + \frac{2}{3}f_1'}{1 + 2f_1}\right)^{\frac{1}{2}} \frac{4\pi^2 T^2 \Gamma_G^2}{E_G^5}\ . \qquad (19)$$

Figure 7 illustrates the important property of this model that the strength function depends on the temperature, T (and therefore on the capture or final state energy), as well as the transition energy.

As $E_\gamma \to E_G$, the denominator diverges, and Eq. (18) fails badly. On the other hand, if the limiting value of Eq.

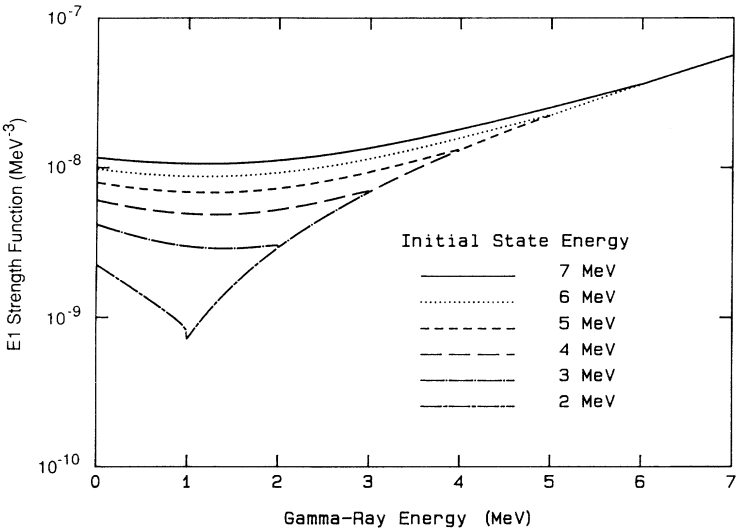

FIG. 7. An illustration of the modification of Brink's hypothesis in the model of Kadmenskij ($E1$-c). The strength function is seen to depend not only on the transition energy, but also on the initial state energy. The apparent cusp in the lowest curve shown is the consequence of an abrupt change of the nuclear temperature at an excitation corresponding to the backshift parameter Δ.

(19) is added to the expression of Eq. (16), the modified formula gives results similar to Eq. (18) for low-energy transitions from highly excited initial states, but in contrast to Eq. (18), is valid for $E_\gamma \to E_G$. This modified Lorentzian proposed by Chrien [24] has been therefore used in analyses of primary transitions proceeding from states near neutron binding energy. However, it can be easily shown that for low-energy transitions between low-lying states this modification of Eq. (16) is not justified. For this reason we use the original expression given by Eq. (18), in spite of the fact that it is not accurate for energies E_γ close to the giant resonance energy.

($E1$-d) The modified formula by Kadmenskij *et al.* fulfilling Brink's hypothesis.

As is evident from previous analyses, involving a number of (n,γ) reactions at isolated neutron resonances, the experimental data on primary $E1$ transitions are in good agreement with a description of the photon strength function based on modified Lorentzian forms described above. Although such strength functions depend on temperature T in the final state E_f, the observed agreement cannot be regarded as decisive evidence for a modification of Brink's hypothesis. Indeed, considering experimental data on primary transitions, it can be easily shown that the same agreement would be observed in the case of an $E1$ strength function, say, $\widetilde{S}_{E1}(E_\gamma)$, defined by

$$\widetilde{S}_{E1}(E_\gamma) = S_{E1}(E_\gamma, T = f^{-1}(E_\gamma)) \ , \tag{20}$$

where $S_{E1}(E_\gamma,T)$ is the photon strength function following from the modified Lorentzian and $f^{-1}(E_\gamma)$ is the function inverse to

$$f(T) = -aT^2 + T + B_n - \Delta \ . \tag{21}$$

In other words, $\widetilde{S}_{E1}(E_\gamma)$ is identical with $S_{E1}(E_\gamma,T)$ for the initial state at the neutron binding energy, and keeps this form for each initial state energy.

Direct evidence of a modification of Brink's hypothesis can only be based on a comparison to intensities of transitions with a fixed energy E_γ and a variable final state energy. In an explicit form no information on such intensities is so far available. However, in view of the fact that in cascade decay of a capturing state the second step may connect various initial and final states, the needed information is implicitly contained in the TSC spectra.

It seems therefore that these spectra can be employed to test the validity of Brink's hypothesis. For this reason the strength function following Eq. (18) with $T = f^{-1}(E_\gamma)$ according to Eq. (21) has also been used in our analysis.

($E1$-e) The model by Sirotkin [11]

$$S_{E1}(E_\gamma,T) = \frac{E_G^6}{4\pi^2 E_0^2 \Gamma_G^2 T_c^3}\, S_0 E_\gamma (E_\gamma^2 + E_0^2) \frac{\Gamma_G \Gamma(E_\gamma,T)}{(E_\gamma^2 - E_G^2)^2} \times \frac{1}{1-\exp(-E_\gamma/T)} \ , \tag{22}$$

where S_0 is the limit of the strength function at $E_\gamma \to 0$ for the initial state at the neutron threshold, E_0 is a typical energy of particle-hole transitions, and T_c is the temperature corresponding to the neutron threshold. This parametrization is not identical with that originally used but it is more convenient for a comparison with neutron capture data. Equation (22) results from different approximations than those of Eq. (18), but it is also based on the theory of Fermi liquids. It can, however, be used only for $E_\gamma \ll E_G$.

In accordance with the Fermi liquid model [25] we take

$$E_G^2 = 1.4\ E_0^2 \ .$$

Following the recommendation of Sirotkin [11] we fix

$$S_0 = 0.5 \times 10^{-8}\ \mathrm{MeV}^{-3} \ .$$

2. $M1$ radiation

Very little information about $M1$ strengths in the ^{144}Nd nucleus is as yet available. We have employed only two simple models.

($M1$-a) The single-particle model. The energy-independent strength S_{M1} has been used as a free parameter. The values tested in the fitting procedure are based on some experimental data for primary $M1$ transitions from neutron capturing states [6]. The experimental value for the target ^{143}Nd corresponds to $S_{M1} = (0.3 \pm 0.2) \times 10^{-8}$ MeV^{-3}, and is considerably below the global average reported in that survey.

($M1$-b) The standard Lorentzian. We have represented $S_{M1}(E_\gamma)$ by the right-hand side of Eq. (15), where we have taken the parameters from Ref. [18],

$\sigma_0 = 0.37$ mb,

$E_G = 7.82$ MeV,

$\Gamma_G = 4.00$ MeV.

3. $E2$ radiation

Transitions of $E2$ type have a very small influence to the resulting effect on two-step cascades. We have used the simple single-particle model with

$S_{E2} = 0.4 \times 10^{-10}$ MeV^{-5}.

VI. RESULTS AND DISCUSSION

Using the models described previously, we have calculated the expected values of integrated TSC intensities in TSC spectra for the five known low-lying states of the ^{144}Nd nucleus. In addition, we have calculated the corresponding values for the average total radiative widths for the capturing states.

The parameter S_{M1} of the single-particle $M1$ strength function has been varied to satisfy two conditions, sometimes contradictory: to fit the experimental value of the average total radiation width for neutron s resonances, and the values of integrated TSC intensities. The reported experimental value for the $M1$ strength $(0.3 \pm 0.2) \times 10^{-8}$ MeV^{-3} [6] places only a loose constraint on the choice of models, and we allow a range of values consistent with that constraint. For model ($E1$-a) we have put $S_{M1} = 0.3 \times 10^{-8}$ MeV^{-3}, for ($E1$-b) $S_{M1} = 0.3 \times 10^{-8}$ MeV^{-3}, for ($E1$-c) and ($E1$-d) $S_{M1} = 0.4 \times 10^{-8}$ MeV^{-3}, and for ($E1$-e) $S_{M1} = 0.5 \times 10^{-8}$ MeV^{-3}.

The integrated TSC intensities calculated for these models for photon strength functions are compared with those obtained experimentally in Figs. 8(a)–8(e). For each figure, the electric dipole model is paired with single-particle and giant resonance models for the magnetic dipole component. Three-step cascade contributions resulting from model calculations are shown separately. For each fit, a goodness of fit parameter, calculated in the manner of a χ^2 per degree of freedom, has been calculated to give a quantitative impression of the relative success in modeling the intensities. These are as follows: (a) 25.9 and 41.7; (b) 1.3 and 5.4; (c) 2.8 and 24.9; (d) 8.2 and

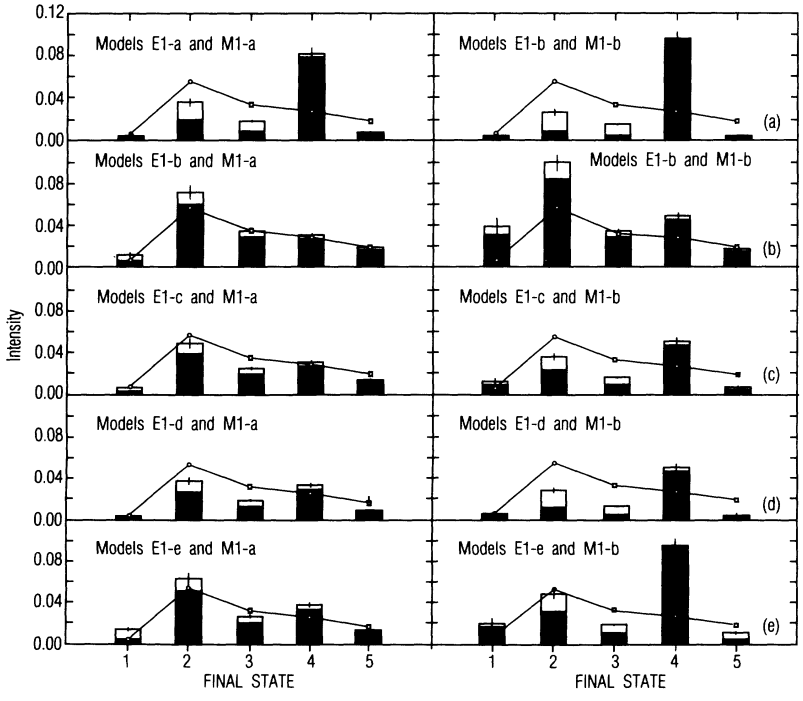

FIG. 8. Calculated TSC intensities compared to experiment for five ^{144}Nd final states: (a) 0^+ ground state, (b) 2^+ 696 keV, (c) 4^+ 1314 keV, (d) 3^- 1510 keV, and (e) 2^+ 1561 keV excited states. Error bars represent Porter-Thomas fluctuations in the model and experimental uncertainties for the data. An overall normalization uncertainty is not shown. The calculated two-step intensities are shown by shaded bars, the three-step intensities by open bars. The experimental data are shown as points connected by line segments. The models ($E1$-a) through ($E1$-e), as described in the text, are paired with the models ($M1$-a) and ($M1$-b). The level density model (LD-a) is used with all models except for the pairs ($E1$-b),($M1$-b) and ($E1$-e),($M1$-a).

TABLE I. Average total radiation widths (in meV) of s-wave resonances at the neutron binding energy calculated using the same models as in Figs. 10–14. The experimental value is 80 ± 9 meV.

Model	($E1$-a)	($E1$-b)	($E1$-c),($E1$-d)	($E1$-e)
($M1$-a)	190.2 ± 4.4[a]	31.3 ± 0.8[a]	$82.7\pm$[a]	134.6 ± 4.5[b]
($M1$-b)	179.4 ± 4.4[a]	24.8 ± 0.7[b]	67.6 ± 1.3[a]	135.2 ± 5.6[a]

[a] The level density (LD-a).
[b] The level density (LD-b).

39.8; and (e) 3.3 and 19.3 per degree of freedom, respectively. It should be emphasized here that this goodness of fit is not a precise expression of a statistically valid χ^2, because the cascades are partially correlated in a rather complicated way.

Average total radiation widths $\overline{\Gamma}_\gamma$ of s-neutron capturing states near the neutron binding energy B_n are given in Table I. They were calculated from the expression

$$\overline{\Gamma}_\gamma = \frac{\rho(3^-, B_n)\overline{\Gamma}_\gamma(3^-, B_n) + \rho(4^-, B_n)\overline{\Gamma}_\gamma(4^-, B_n)}{\rho(3^-, B_n) + \rho(4^-, B_n)} \tag{23}$$

for the same models as in the case of integrated TSC intensities. In Eq. (23) both possible spins and parities 3^- and 4^- of s-neutron capturing states in the ^{144}Nd nucleus are taken into account. The experimental total radiation width has the average value 80 ± 9 meV [26]. The results in Table I agree with those obtained previously (for different level densities) [18]: The classical Lorentzian ($E1$-a), as expected, strongly overestimates radiation widths while the Lorentzian with the energy- and temperature-dependent damping width ($E1$-b) gives values which are too small. On the other hand, good agreement with the experimental value is observed in the model by Kadmenskij *et al.* ($E1$-c).

Integrated TSC intensities obtained by modeling strongly differ from those obtained experimentally for the standard Lorentzian ($E1$-a) and for model ($E1$-d) for the $E1$ strength function. A relatively good agreement was reached for models ($E1$-b), ($E1$-c), and ($E1$-e) of the $E1$ strength function combined with the single-particle model of the $M1$ strength function. The best results are obtained in the case of models ($E1$-b) and ($E1$-c), but all models of the $E1$ strength function which incorporate a temperature-dependent spreading width give a reasonable agreement with experiment. Therefore, the specific form of the energy and temperature dependence of the damping width given by Eq. (17), which is common for all these strength functions, seems to be crucial for the explanation of the TSC intensity behavior.

In our opinion, the strongest argument for the need for a modification of Brink's hypothesis is the fact that the formula by Kadmenskij *et al.* ($E1$-c) reproduces experimental integrated TSC intensities, whereas the modified formula ($E1$-d) does not.

A closer inspection of Fig. 8 reveals that an important role in testing various models is played by the integrated TSC intensity in the spectrum for the 3^- state at 1510 keV. Generally, the TSC intensity should depend on the excitation energy, the spin, and the parity of the final state. Plausible assumptions lead to the expectation that if $S_{E1} \approx S_{M1}$ at energies $E_\gamma \approx 3$ or 4 MeV, the integrated TSC intensity does not depend on the parity π_f of the final state. On the other hand, for S_{E1} significantly greater than S_{M1}, the intensity of two-step cascades ending at states with $\pi_f = \pi_c$ will be enhanced (whereas the three-step cascades intensity will be reduced) in comparison with states with $\pi_f = -\pi_c$. This important feature differentiates the method of two-step cascades from previous methods, which are sensitive mostly to the sum $S_{E1} + S_{M1}$. The effect is seen clearly in Fig. 8(a) because the standard Lorentzian form, with an invariant and large width, ensures the dominance of $E1$ strength at all excitations.

The conclusion that the single-particle model $M1$ strength function fits the integrated TSC intensities better than the standard Lorentzian is in contradiction with previous results [18, 19]. However, we note that both $M1$ strength function models employed are rather unrealistic and we do not regard this contradiction as very meaningful. Indeed, the fact that all models overestimate the integrated TSC intensity in the case of the 3^- state shows that their ratios S_{E1}/S_{M1} cannot be fully correct. The behavior observed may indicate a need for a more realistic formula for the $M1$ strength function.

VII. CONCLUSION

The results of this experiment are in reasonable agreement with earlier information on the $E1$ strength function. The model with an energy- and temperature-dependent damping width and with a nonzero limit at $E_\gamma \to 0$ explains most of the data on spherical and transitional nuclei, including those from this experiment. In addition, evidence of a significant modification of Brink's hypothesis for the $E1$ strength function was presented.

In spite of uncertainties associated with Porter-Thomas fluctuations, experimental errors, and correlations in the TSC intensities, departures of the integrated TSC intensities from those resulting from modeling are statistically meaningful. The method of two-step cascades represents a useful tool and experiments similar to this should be repeated for other nuclei. In particular, we propose to use this method for deformed nuclei, for which new data on photon strength functions are in great demand.

ACKNOWLEDGMENTS

This research was supported in part by Charles University and the U.S. Department of Energy under Contract No. DE-AC02-76CH00016. The authors wish to thank the technicians and operating crew of the BNL High Flux Beam Reactor for their assistance. One of us (F. B.) wishes to express his gratitude to Brookhaven National Laboratory and its staff for their hospitality and financial support during the duration of the experiment.

[1] G.C. Baldwin and G.S. Klaiber, Phys. Rev. **73**, 1156 (1948).
[2] M. Goldhaber and E. Teller, Phys. Rev. **74**, 1046 (1948)
[3] D.M. Brink, Ph.D. thesis, Oxford University, 1955.
[4] G.A. Bartholomew, E.D. Earle, A.J. Ferguson, J.W. Knowles, and M.A. Lone, Adv. Nucl. Phys. **7**, 229 (1973).
[5] C.B. Dover, R.H. Lemmer, and F.J.W. Hahne, Ann. Phys. (N.Y.) **70**, 458 (1972).
[6] C. McCullagh, M. Stelts, and R. Chrien, Phys. Rev. C **23**, 1394 (1982).
[7] L. Aldea, B. Kardon, O.W.B. Schult, H. Seyfarth, and N. Wüst, Z. Phys. A **283**, 391 (1977).
[8] W. Furman, K. Niedwiedziuk, Yu.P. Popov, R. Rumi, V. Salatski, V. Tishin, and P. Winiwarter, Phys. Lett. **44B**, 464 (1973).
[9] S.G. Kadmenskij, V.P. Markushev, and V.I. Furman, Yad. Fiz. **37**, 277 (1983) [Sov. J. Nucl. Phys. **37**, 165 (1983)].
[10] D.F. Zaretskij and V.K. Sirotkin, Yad. Fiz. **27**, 1534 (1978) [Sov. J. Nucl. Phys. **27**, 808 (1978)].
[11] V.K. Sirotkin, Yad. Fiz. **43**, 570 (1986) [Sov. J. Nucl. Phys. **43**, 362 (1986)].
[12] A.M. Hoogenboom, Nucl. Instrum. Methods **3**, 57 (1958).
[13] Yu.P. Popov, in *Capture Gamma-Ray Spectroscopy*, Proceedings of the Seventh International Symposium on Capture Gamma-Ray Spectroscopy and Related Topics, Pacific Grove, 1990, edited by R.W. Hoff, AIP Conf. Proc. No. 238 (AIP, New York, 1991), p. 607.
[14] B. Krusche, K.P. Lieb, H. Daniel, T. Von Egidy, G. Barreau, H.G. Borner, R. Brissot, C. Hofmeyr, and R. Rascher, Nucl. Phys. **A386**, 245 (1982).
[15] A.A. Bogzdel *et al.*, JINR Report No. P15-82-706, Dubna, 1982 (unpublished).
[16] W. Dilg, W. Schantl, H. Vonach, and M. Uhl, Nucl. Phys. **A217**, 269 (1973).
[17] J.M. Lang and K.J. Le Couteur, Proc. Phys. Soc. **A67**, 586 (1954).
[18] J. Kopecky and M. Uhl, Phys. Rev. C **41**, 1941 (1990).
[19] J. Kopecky and M. Uhl, in *Capture Gamma-Ray Spectroscopy* [13], p. 607.
[20] F. Bečvář, P. Cejnar, R.E. Chrien, and J. Kopecky, in *Capture Gamma-Ray Spectroscopy* [13], p. 287.
[21] S.F. Mughabghab and D.I. Garber, BNL Report No. BNL325, 1973, Vol. 1, Part A. The most recent compilation [S.F. Mughabghab, M. Divadeenam, and N. E. Holden, *Neutron Cross Sections* (Academic, New York, 1981)] has an error in the listed resonance spacing for ^{143}Nd (private communication, Mughaghab to Chrien, 1991).
[22] B.L. Berman and S.C. Fultz, Rev. Mod. Phys. **47**, 713 (1975).
[23] J. Kopecky and R.E. Chrien, Nucl. Phys. **A468**, 285 (1987).
[24] R.E. Chrien, in *Proceedings of the Vth International School on Neutron Physics, Alushta, Dubna, 1987*, edited by B. B. Kolesova and V. R. Sarantseva (Dubna Report No. D3,4, 17-86-747, 1987).
[25] A.B. Migdal, *Teoriya konechnykh fermi-sistem* (Mir, Moscow, 1967).
[26] S.F. Mughabghab, M. Divadeenam, and N.E. Holden, *Neutron Cross Sections* (Academic, New York, 1981), Vol. 1, Part A.
[27] S. Raman (private communication to Carol McCullagh, 1979).